Yassir EL KARKRI [1,*], Hassane EL MARKHI [1], Hassan EL MOUSSAOU[1], Tijani LAMHAMDI[1]

J. Electrical Systems 14-4 (2018): 1-20

Regular paper

Journal of Electrical Systems

LVRT and HVRT control strategies of Doubly-Fed Induction Generator

The Doubly Fed Induction Generator (DFIG) has a high sensitivity to the Grid Faults (GFs), which can cause many problems on the power quality and the production continuity. Actually, the grid connection requirements impose strict laws to respect to Low Voltage Ride Through (LVRT), High Voltage Ride Through (HVRT), and grid support capacities following the Grid Codes (GCs). In fact, when detecting voltage fault, Wind Turbines (WTs) should stay in connection with the grid in order to hold a safe and stable operation. The main objective of this work is to propose LVRT and HVRT strategies able to retain WTs connected to the grid during severe grid voltage faults. The proposed approach is a hybrid method combining two methods (active and passive methods): The first aim is to develop the control of DFIG, while the second is applied for severe voltage faults using hardware protection circuits.

Keywords: DFIG; HVRT; LVRT; Active method; Passive method.

Article history: Received 24 April 2018, Accepted 30 September 2018

1. Introduction

Renewable power sources have grown quickly among the latest couple of years due to the augmentation in demand for the electrical power and with a specific end goal to diminish fossil resources which can injure the nature [1]. There are diverse assets of the renewable power source, in this paper, we are occupied with wind energy which is viewed as the most oftentimes used to their relatively minimal cost, low upkeep and clean contrasted with other renewable power sources [2-3].

As wind power potential has amplified, so has the necessity for wind farms to become more dynamic in keeping the grid safety and power quality of the grid [4-6]. This raised situation into the power-market drives us to serious questions about its capacity to provide ancillary services, such as the imbalance and loss compensation, thus the voltage-frequency regulation during GF. In this conditions, Grid Operators (GOs) are getting to be plainly stricter with the utilization of wind power as far as their behavior compared to traditional power sources [4]. This limited utilization of wind power sources is executed through a continuous refreshing of their GCs [7-9]. Where the technical conditions requested for wind power plants are stricter, or much more critical, than those for conventional energy sources [10]. The GCs technical specifications are classified into two categories: (i) static and (ii) dynamic requirements. The static requirements talk about the steady-state behavior and the power quality at the connection point to the grid [9]. While the dynamic obligations concern the desired WT generator response during fault times. Usually, these requirements cover many subjects such as voltage operation range, control of power factor, frequency operation range, and fault ride through [11]. Moreover, the value of DFIG based WTs is becoming more and more important as it is appropriate for advanced features accomplishment implementing required for grid integration [12]. DFIG grants some profits, such as reduced costs of power-inverter and output filter due to low power conversion ratings of rotor and grid sides (25%–30%) [13-15], However, WTs based on DFIG are so delicate to grid disturbances, especially to Voltage Dips (VDs) and Voltage Swells (VSs) [16-18].

[*1] Corresponding author: EL KARKRI Yassir, The Signals, Systems, and Components Laboratory, Sidi Mohamed Ben Abdellah University, FST Fez, 30000, Morocco, E-mail: yassir.elkarkri@usmba.ac.ma

GCs requirements mostly apply to wind farms connected to the transmission lines. These GCs indicate that wind farms should keep the power system control, and assert wind farm behavior in case of irregular functioning states of the grid (in case of VDs and VSs). The several general requirements introduce Faults Ride Through (FRT) capability, active power control, frequency control, and power factor regulation abilities [19]. The typical GCs principal requirements are given below:

- Frequency functioning area: Wind farms are obliged to operate continuously within usual grid frequency variations.
- Active power: Wind farms must have the capacity to control their active power in order to guarantee a stable operating and to prevent overloading of the grid and to diminish the effect of dynamic WT operation through extreme wind conditions.
- Reactive power: Wind farms should remain the reactive power stability and kept the power factor in the desired area.
- LVRT and HVRT: During grid voltage faults, WTs are required to rest connected for a specific time before being allowed to disconnect. This requirement is to guarantee that there is no generation loss for normally cleared faults. Disconnecting a WT rapidly could have a negative impact on the grid, particularly for big wind farms. GCs require that WTs must resist voltage variation at a specified rate of the nominal voltage and for a specified duration. Such constraints are known as LVRT (for VDs) and HVRT (for VSs). They are represented by a voltage (u) versus time (t) characteristic, indicating the minimum required protection of the wind power farms to the system voltage variations (Figure 1 and 2) [10].

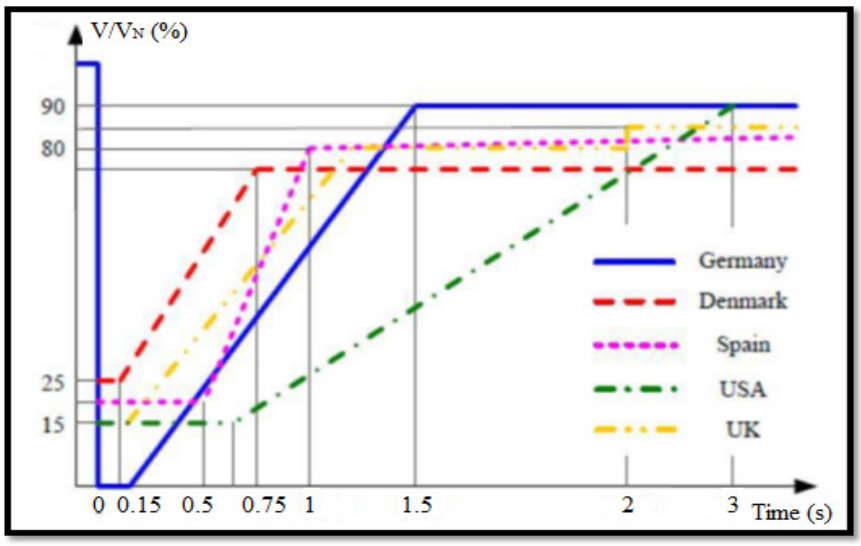

Figure 1: LVRT requirements.

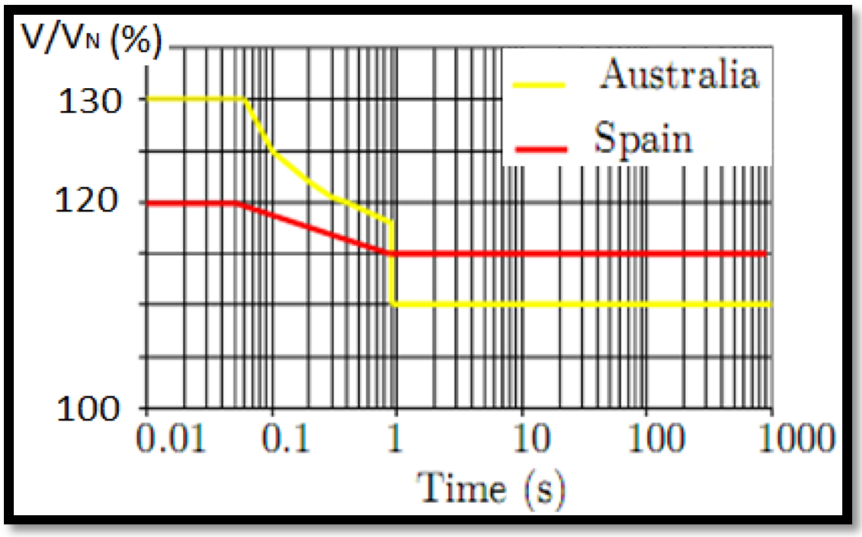

Figure 2: HVRT requirements.

Diverse studies discussed in the literature have addressed the LVRT and HVRT capability for DFIGs.

These strategies can be classified into two principal categories:

- Active methods: using appropriate converter control.
- Passive methods: using an additional electronic equipment.

For the active methods, the conventional solution for FRT requirements is the use of the crowbar circuit [20-22]. Despite the fact that the crowbar circuit protection is a cost-effective strategy, capable to secure the power converters of DFIG, its disadvantage is that the DFIG misses its controllability once the crowbar circuit is activated, due to the Rotor Side Converter (RSC) deactivating. In such condition, DFIG consumes reactive power from the grid because of Grid Voltage (GV) degradation. In the same context, a Stator Damping Resistor (SDR) composed of three resistors and three bypassing bidirectional switches coupled in series with the stator circuit is proposed in [23]. In normal states, these switches rest closed and the stator current will not circle within the resistors. The LVRT methods seem to be more effective than those using conventional crowbar circuit. In addition, using these approaches, it seems possible to enhance DFIG FRT capability as the main disadvantage of the crowbar is missing the DFIG control over GFs [24]. Also, an Energy Storage System (ESS) proposed in [25] can help to stabilize the DC-voltage and mitigate the output power simultaneously, but it is very difficult to diminish the electromagnetic torque oscillations and rotor overcurrent.

In the other hand, for passive methods, it has also been proposed combination of control strategies and the addition of electronic components [26-27]. A transient current control scheme is proposed for the RSC with crowbar protection in [28]. A different solution is proposed on [27] by utilizing a Parallel Grid Side Rectifier (PGSR) with a Series Grid Side Converter (SGSC). This converters combination allows unrestricted power processing and robust control of voltage changes.

Some researchers add an external power electronic device called a Dynamic Voltage Restorer (DVR), is an electrical voltage converter connected to the grid in order to compensate voltage variation. Different DVR Shapes are proposed to protect the DFIG WT in [29-31], but the control of reactive power during GFs is not considered. In [32] and [33] the authors proposed strategies to compensate the VS using Static Synchronous Compensator (STATCOM) and DVR devices. However, these strategies need additional electrical devices which augment the system complexity.

In this paper, we propose a control strategy to develop the LVRT and HVRT capability of the DFIG during symmetrical grid voltage faults. The proposed strategy for LVRT combines

the active method to limit fault in current at low VDs and the passive method for severe VDs by adding hardware protections like SBR. The proposed solution for HVRT capability involves the use of DVR to maintain DFIG terminal voltage stable and to provide maximum support to help the GV fast recovery by controlling power converters.

This paper is structured as: In the second section, the modelling and control of DFIG based WTs are presented. In the third section, the DFIG behavior during symmetrical grid voltage faults is analyzed. In the fourth section, the proposed LVRT and HVRT strategies are presented. The Fifth section presents the simulation results of the proposed strategies compared with the system without LVRT and HVRT strategies. Finally, the conclusion is summarized in the sixth section.

2. DFIG modelling and control

The electrical part of DFIG consists of stator windings which are directly related to the three-winding transformer, while the machine's rotor windings are directly excited by an AC/DC/AC power converter. The grid side of the power converter supplies the rotor power into the grid via the three-winding transformer. The DFIG system is represented in Figure 3. The control of the rotor voltages makes it possible to manage the magnetic field inside the machine.

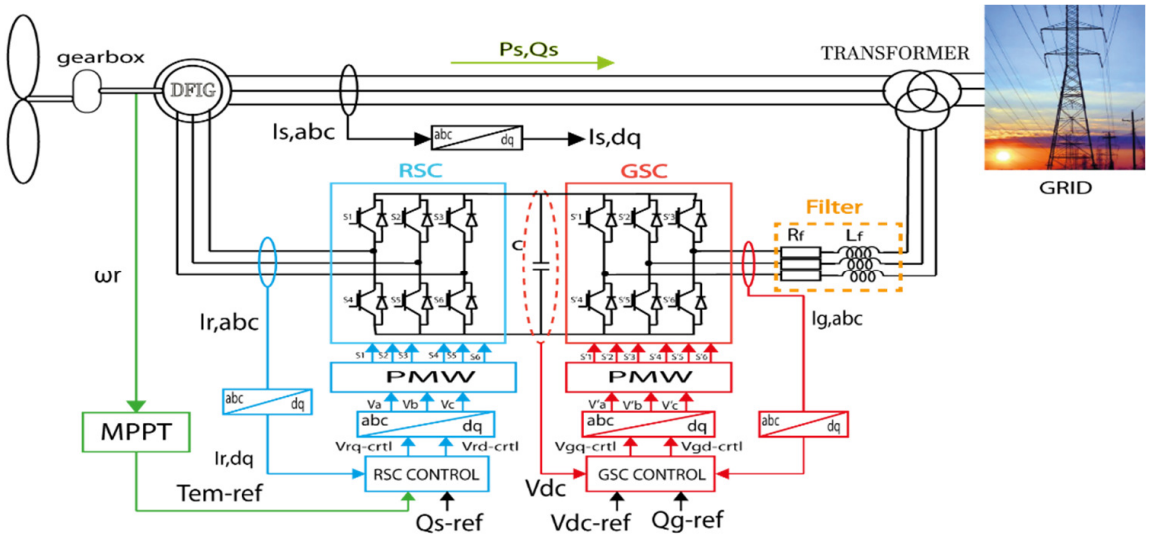

Figure 3: DFIG based WTs representation.

Each winding can be represented by an equivalent electric circuit, according to figure 4 :

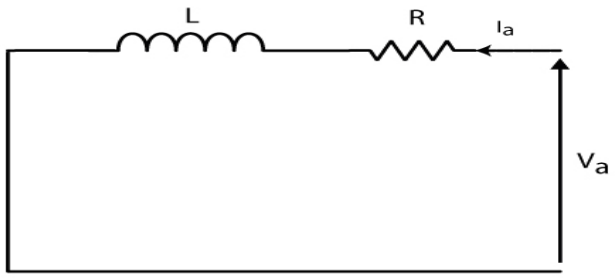

Figure 4: The equivalent circuit for a winding.

The electromotive force developed in the inductance can be expressed by:

$$-e = \frac{d\varphi}{dt} = V_a - RI_a \quad (1)$$

By applying the mesh law to the three stator windings, we obtain:

$$\begin{bmatrix} v_{sa} \\ v_{sb} \\ v_{sc} \end{bmatrix} = \begin{bmatrix} R_S & 0 & 0 \\ 0 & R_S & 0 \\ 0 & 0 & R_S \end{bmatrix} \begin{bmatrix} I_{sa} \\ I_{sb} \\ I_{sc} \end{bmatrix} + \frac{d}{dt} \begin{bmatrix} \phi_{sa} \\ \phi_{sb} \\ \phi_{sc} \end{bmatrix} \quad (2)$$

A similar relation is obtained for the three windings of the rotor:

$$\begin{bmatrix} v_{ra} \\ v_{rb} \\ v_{rc} \end{bmatrix} = \begin{bmatrix} R_r & 0 & 0 \\ 0 & R_r & 0 \\ 0 & 0 & R_r \end{bmatrix} \begin{bmatrix} I_{ra} \\ I_{rb} \\ I_{rc} \end{bmatrix} + \frac{d}{dt} \begin{bmatrix} \phi_{ra} \\ \phi_{rb} \\ \phi_{rc} \end{bmatrix} \quad (3)$$

In the absence of saturation, the flux is assumed to be linearly dependent on the currents. The total flux in each winding is given by the sum of the flux from the self-inductance, the flux linked by the mutual inductances for a stator winding, and the flux linked to variable mutual inductance according to the rotor position.

The equations of flux in a matrix form are:

$$\begin{bmatrix} \phi_{sa} \\ \phi_{sb} \\ \phi_{sc} \end{bmatrix} = \begin{bmatrix} l_s & M_s & M_s \\ M_s & l_s & M_s \\ M_s & M_s & l_s \end{bmatrix} \begin{bmatrix} I_{sa} \\ I_{sb} \\ I_{sc} \end{bmatrix} + M[R(\theta)] \begin{bmatrix} I_{ra} \\ I_{rb} \\ I_{rc} \end{bmatrix} \quad (4)$$

$$\begin{bmatrix} \phi_{ra} \\ \phi_{rb} \\ \phi_{rc} \end{bmatrix} = \begin{bmatrix} l_r & M_r & M_r \\ M_r & l_r & M_r \\ M_r & M_r & l_r \end{bmatrix} \begin{bmatrix} I_{ra} \\ I_{rb} \\ I_{rc} \end{bmatrix} + M[R(\theta)] \begin{bmatrix} I_{sa} \\ I_{sb} \\ I_{sc} \end{bmatrix} \quad (5)$$

Ms and Mr are respectively the mutual inductances between two stator and rotor phases.

l_s And l_r are respectively the own inductances of a stator and rotor windings.

With

$$[R(\theta)] = \begin{bmatrix} \cos(\theta) & \cos(\theta - \frac{2\pi}{3}) & \cos(\theta + \frac{2\pi}{3}) \\ \cos(\theta + \frac{2\pi}{3}) & \cos(\theta) & \cos(\theta - \frac{2\pi}{3}) \\ \cos(\theta - \frac{2\pi}{3}) & \cos(\theta + \frac{2\pi}{3}) & \cos(\theta) \end{bmatrix} \quad (6)$$

To represent effectively the behavior of a DFIG, and reduce the complexity, it is necessary to use a precise and sufficiently simple model. Instead of considering the three fixed phases (sa, sb, sc) of the stator and (ra, rb, rc) three phases windings of the machine's rotor, we consider the equivalent diagram formed of two component (d: direct and q: quadrature) by applying the park transformation, as shown in Figure 5.

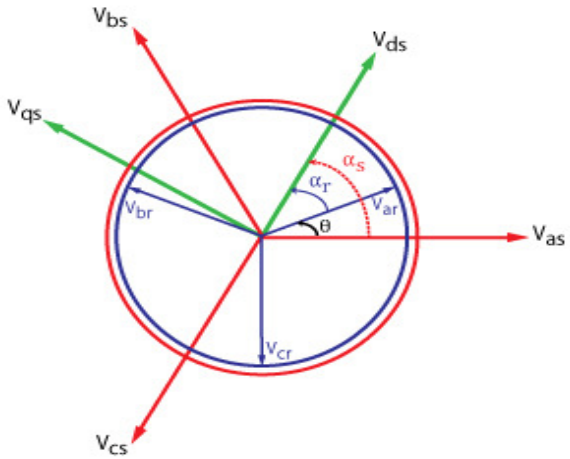

Figure 5: DFIG Park model for stator voltage.

The new model is obtained by multiplying the equations of currents, flows, and voltages by the Park matrix given by the following equation:

$$P[\alpha] = \begin{bmatrix} \cos(\alpha) & \cos(\alpha - \frac{2\pi}{3}) & \cos(\alpha + \frac{2\pi}{3}) \\ -\sin(\alpha) & -\sin(\alpha - \frac{2\pi}{3}) & -\sin(\alpha + \frac{2\pi}{3}) \end{bmatrix} \quad (7)$$

The change of variables relating to (currents, voltages, and flux) is defined by the following transformation:

$$\begin{bmatrix} X_d \\ X_q \end{bmatrix} = P[\alpha] \begin{bmatrix} X_a \\ X_b \\ X_c \end{bmatrix} \quad (8)$$

To determine the angles required for Park transformations for stator magnitudes (αs) and rotor magnitudes (αr), a Phase-Locked Loop (PLL) is used. This PLL makes it possible to estimate with precision the frequency and the amplitude of the GV.

After the Park transformation application to equations (2), (3), (4), and (5), and with a reference linked to the rotating field, the expression of the stator and rotor voltages along the d-q axis are expressed by:

$$\begin{cases} V_{sd} = R_s I_{sd} + \frac{d\varphi_{sd}}{dt} - \omega_s \varphi_{sq} \\ V_{sq} = R_s I_{sq} + \frac{d\varphi_{sq}}{dt} + \omega_s \varphi_{sd} \\ V_{rd} = R_r I_{rd} + \frac{d\varphi_{rd}}{dt} - \omega_r \varphi_{rq} \\ V_{rq} = R_r I_{rq} + \frac{d\varphi_{rq}}{dt} + \omega_r \varphi_{rd} \end{cases} \quad (9)$$

With: $\omega_s = \frac{d\theta_s}{dt}$ is the stator pulsation and $\omega_r = \frac{d\theta_r}{dt}$ is the rotor pulsation.

The matrix flux system can be expressed as follows:

$$\begin{cases} \phi_{sd} = L_s I_{sd} + MI_{dr} \\ \phi_{sq} = L_s I_{sq} + MI_{qr} \\ \phi_{rd} = L_r I_{rd} + MI_{ds} \\ \phi_{rq} = L_r I_{rq} + MI_{qs} \end{cases} \quad (10)$$

The expression of the electromagnetic torque of DFIG depending on the stator flux and rotor currents is expressed as follows:

$$C_{em} = \frac{M}{L_s}\left(\phi_{sq} I_{dr} - \phi_{sd} I_{rq}\right) \quad (11)$$

The active and reactive power of the DFIG are written as follows:

$$\begin{cases} P_s = 1.5(V_{ds} I_{sd} + v_{qs} I_{qs}) \\ Q_s = 1.5(v_{qs} I_{sd} - v_{ds} I_{qs}) \\ P_r = 1.5(v_{dr} I_{rd} + v_{qr} I_{qr}) \\ Q_r = 1.5(v_{qr} I_{rd} - v_{dr} I_{qr}) \end{cases} \quad (12)$$

In order to simplify DFIG equations, we will now proceed to an orientation choice for PARK reference d-q. In the present work, we will use the vector control method by the orientation of stator voltage (Figure 6), the choice of this reference makes the electromagnetic torque produced by the machine depends on a single component of the current, therefore the active power only depends on the d-axis rotor current and the reactive power depends only on the q-axis rotor current. Thus, these powers can be controlled individually.

The first simplification resulting from the choice of orientation according to the stator flux is:

$$\phi_{sd} = 0 \quad \rightarrow \quad \frac{d\phi_{sd}}{dt} = 0$$

The stator flux is imposed by the grid. Therefore, we can consider ϕ_{sq} as constant (its derivative will be zero) and equal to the modulus of the stator flux vector ϕ_s as represented in the following equation:

$$\begin{cases} \varphi_{sq} = \phi_s \\ \phi_{sd} = 0 \end{cases} \tag{13}$$

It is customary for high power generators used in current WT to neglect the stator resistance Rs, we assume that Rs = 0, the equations of stator voltages become:

$$\begin{cases} V_{sq} = 0 \\ V_{sd} = V_S = -\omega_s \phi_s \end{cases} \tag{14}$$

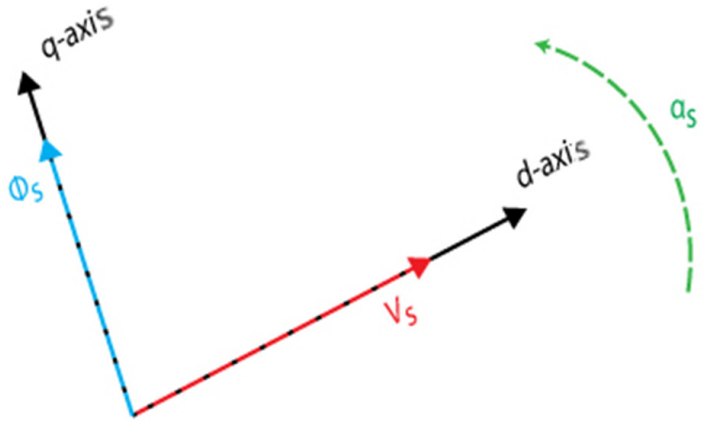

Figure 6: Stator voltage orientation along d-axix.

The electromagnetic torque in equation 11 is written as:

$$C_{em} = \frac{M}{L_s}\left(\phi_{sq} I_{dr}\right) \tag{15}$$

And the equation of the stator fluxes according to (13) becomes:

$$\begin{cases} \varphi_{sq} = \phi_s = L_S I_{sq} + MI_{qr} \\ \phi_{sd} = 0 = L_S I_{sd} + MI_{dr} \end{cases} \tag{16}$$

The reactive power and the active power are written as follows:

$$\begin{cases} Q_s = -\frac{v_s}{L_s}\left(\frac{v_s}{w_s} - MI_{qr}\right) \\ P_s = -\frac{v_s}{L_s}(MI_{dr}) \end{cases} \tag{17}$$

3. DFIG behaviour during grid faults

Without any protection system, the grid system disturbances can lead to large fault currents in the stator windings. Because of the magnetic coupling between the stator windings and the rotor windings, each distress in the stator part is transmitted directly to the rotor circuit. However, the dimensioning of the power converter is relatively small compared to the system, so it would not be possible to keep the controllability of the system for high rotor current. This means that the converter reaches quickly its limits, therefore, it loses control of the generator during the GF. Also, in this conditions the Grid Side Converter (GSC) cannot transfer the power to the grid and therefore the extra energy charges the capacitor, then the DC-link voltage can increase rapidly.

To see the DFIG behaviour, the evolution of its magnitudes during the GFs, and to be able to determine the causes and subsequently to propose solutions, we made a study on DFIG's dynamic response during the grid disturbances.
The stator and rotor voltage equations are expressed by:

$$\overrightarrow{v_s} = R_s\overrightarrow{\imath_s} + \frac{d\overrightarrow{\varphi_s}}{dt} \tag{18}$$

$$\overrightarrow{v_r} = R_r\overrightarrow{\imath_r} + \frac{d\overrightarrow{\varphi_r}}{dt} \tag{19}$$

Stator and rotor flux-linkage expressions are expressed by:

$$\overrightarrow{\phi_s} = L_s\overrightarrow{\imath_s} + M\overrightarrow{\imath_r} \tag{20}$$

$$\overrightarrow{\phi_r} = L_r\overrightarrow{\imath_r} + M\overrightarrow{\imath_s} \tag{21}$$

According to equations (19), (20), and (21) the expression of the rotor voltage becomes:

$$\overrightarrow{v_r} = \overrightarrow{\mathrm{e_r^r}} + (\mathrm{R_r} + \mathrm{L_r}(1 - \frac{M^2}{L_s L_r}\frac{\mathrm{d}}{\mathrm{dt}})\overrightarrow{\mathrm{i_r^r}} \tag{22}$$

With $\overrightarrow{\mathrm{e_r^r}} = \frac{\mathrm{M}}{\mathrm{L_s}}\frac{\mathrm{d}\overrightarrow{\phi_s^r}}{\mathrm{dt}}$ is the electromotive force and $\overrightarrow{\phi_s^r} = \phi_s e^{-jw_r t}$ is the stator flux expressed in a frame linked to the rotor axes.

In normal operation, the stator voltage vector has a fixed amplitude Vs and rotates at the synchronism speed ws:

$$\overrightarrow{v_s} = \mathrm{V_s e^{j\omega_s t}} \tag{23}$$

When a symmetrical fault happens at t=t0, the stator voltage decrease from V_1 à V_2:

$$\overrightarrow{v_s} = \begin{cases} V_1 e^{j\omega_s t} & t < t_0 \\ V_2 e^{j\omega_s t} & t > t_0 \end{cases} \tag{24}$$

The evolution of the flux during the GF is written:

$$\overrightarrow{\phi_s} = \begin{cases} \frac{V_1}{jw_s} e^{j\omega_s t} & t < t_0 \\ \frac{V_2}{jw_s} e^{j\omega_s t} & t > t_0 \end{cases} \tag{25}$$

The flux cannot change from φ1 to another φ2 instantly, there must be continuity, thus to guarantee a progressive change of the flux, a DC component of the flux appears.
Using equation 24 and 25, the stator voltage becomes:

$$\overrightarrow{v_s} = \frac{R_s}{L_s}\overrightarrow{\phi_s} + \frac{d\overrightarrow{\phi_s}}{dt} - \frac{R_s M}{L_s}\overrightarrow{i_r} \tag{26}$$

Considering the low values of the DFIG quantities, the last term can be neglected, we obtain:

$$\overrightarrow{v_s} = \frac{R_s}{L_s}\overrightarrow{\phi_s} + \frac{d\overrightarrow{\phi_s}}{dt} \tag{27}$$

The flux expression is determined by solving the previous differential equation:

$$\overrightarrow{\phi_s} = \frac{V_2}{j\omega_s}e^{j\omega_s t} + \frac{V_1 - V_2}{j\omega_s}e^{-t/\tau_s} \tag{28}$$

With: $\tau_s = \frac{L_s}{R_s}$

Replacing the stator flux with its expression in $\overrightarrow{e_r}$, we find:

$$\overrightarrow{e_r} = \frac{M}{L_s}V_2 g e^{j\omega_{sr}t} - \frac{M}{L_s}\frac{V_1 - V_2}{j\omega_s}(j\omega_r + \frac{1}{\tau_s})e^{-t/\tau_s}e^{-j\omega_r t} \tag{29}$$

By neglecting the term $1/\tau_s$, the preceding equation becomes:

$$\overrightarrow{e_r} = \frac{M}{L_s}V_2 g e^{j\omega_{sr}t} - \frac{M}{L_s}(V_1 - V_2)(1-g)e^{-t/\tau_s}e^{-j\omega_r t} \tag{30}$$

The maximum amplitude of $\overrightarrow{e_r}$ appears at the beginning of the VD:

$$e^r_{r,max} = \frac{M}{L_s}(V_2 g - (V_1 - V_2)(1-g)) \tag{31}$$

It can be seen from the previous expression that e_r^r is the sum of two terms, a term which is proportional to the slip, therefore she has a small amplitude, while the second term its amplitude can be large or small, depending on the depth of the GF $(V_1 - V_2)$. During GF, the appearance of the DC component at the magnetic-flux causes overvoltage in the rotor. If the RSC is unable to control it, overcurrent will appear in the rotor and the converter may be damaged.

4. LVRT and HVRT Control Strategies

The control strategies applied during GFs can be divided into two main categories: LVRT control strategy for VDs and HVRT control strategy for VSs.

4.1 LVRT control strategy

Two control methods are applied for LVRT wind power capacity, depending on the VD level. The first method (active method) is based on the flux control in order to limit rotor overcurrent, this method is valid only for small depths of VDs. While the second method (passive method) requires material protections such as the series resistors to minimize significant VDs effects.

a- Active method:

The principal objective of control during GF is to limit the fault current. The method is simple to implement, based on the control of the rotor flux when a VD is detected. The principle is to control the rotor flux during grid VDs to follow the stator flux. Thus, rotor overcurrent can be definitely reduced.

According to equations (20) and (21), and considering that $\frac{L_s}{M} \approx 1$, the rotor current can be expressed by:

$$\overrightarrow{i_r} = \frac{M}{L_s L_r - M^2}(\vec{\phi}_r - \vec{\phi}_s) \tag{32}$$

When the voltage drop occurs, DC component appears in the stator flux, therefore, the rotor flux cannot follow the stator flux. Thus, the difference between the rotor and stator flux

will increase during a VD, which gave rise to rotor overcurrent. For this reason, in order to limit this failure, the rotor flux must be controlled to follow the stator flux.
The rotor flux reference is determined by:

$$\phi_{r,ref} = k_T \phi_s \tag{33}$$

With $0 < k_T < 1$

The expressions of the rotor current are obtained by substituting equation (33) in (32):

$$\overrightarrow{I_r} \simeq \frac{M(k_T - 1)}{L_s L_r - M^2} \overrightarrow{\phi_s} \tag{34}$$

When the fault occurs, the stator flux at t=0 is maximum. If the rotor current is within the limits for the maximum stator flux, it will surely not exceed the maximum of the current during GF, thus k_T should satisfy:

$$\left| \frac{M(k_{T,min} - 1)}{L_S L_R - M^2} \phi_s(0) \right| \leq \left| I_{r_{max}} \right| \tag{35}$$

The expression of $k_{T,min}$ is expressed by:

$$k_{T,min} \simeq 1 - I_{r\_max} \omega_s \frac{(L_s L_r - M^2)}{M V_S} \tag{36}$$

Unfortunately, maintaining production during the disturbed regime of the proposed control is limited because of small dimensioning of the power converters compared to the general system. The activation of this strategy is affected by the severity of the fault, which is why we have studied the feasibility of the proposed strategy against VDs. The maximum amplitude is proved theoretically, while the maximum operation time is obtained by simulation-test [8].

Substituting the flux equation (24) in the expression of reactive power (12) the expression of the reactive power during the fault becomes:

$$\overrightarrow{Q_s} = 1.5 \frac{M}{L_s L_r - M^2} (1 - k_t) [\frac{pV_s}{j\omega_s} e^{j\omega_s t} + \frac{(1-p)V_s}{j\omega_s} e^{-\frac{t}{\tau s}}] v_s \tag{37}$$

With p it is the degree of VD relative to its nominal value

Assuming that the VD occurs at t = 0s, the expression (37) becomes:

$$Q_s(t = 0) = -1.5 \frac{M}{L_s L_r - M^2} (1 - k_t) \frac{(p){V_s}^2}{j\omega_s} \tag{38}$$

$Q_s(t = 0) < 0.3 \implies p > 0.6998 \approx 0.7$

Therefore the modified control strategy remains valid for VDs lower than 30%.

The following table illustrates the operating extremes of the active strategy, at the amplitude and duration levels of VDs to verify its compatibility with existing grid codes represented in Figure 1.

Table 1: The compatibility of the active method with the GCs [8].

Voltage dip level	Duration	Grid codes
30%	0.3s	---
25%	1s	Spain – Danemark-UK
23%	1.5s	Spain – Danemark-UK-Allemand
<23%	>1.5s	Spain – Danemark-UK-Allemand

b- Passive method

The passive method consists of inserting resistors in series with stator windings (SBR), as is represented in Figure 7, to increase the stator voltage and subsequently reduce the DC

component at flux level. This would reduce overvoltage at the rotor circuit and therefore avoid rotor current peaks.

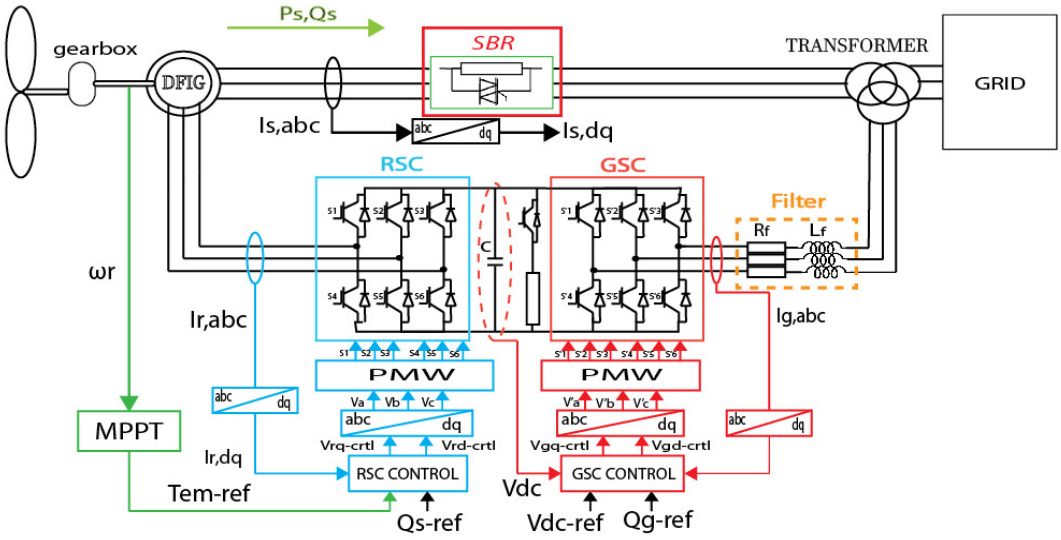

Figure 7: DFIG coupled with SBR.

In addition, the limitation of the rotor current can also reduce overvoltage at Vdc which could damage the power converter. The stator voltage during fault becomes the sum of the GV and the voltage across the resistors (Figure 8):

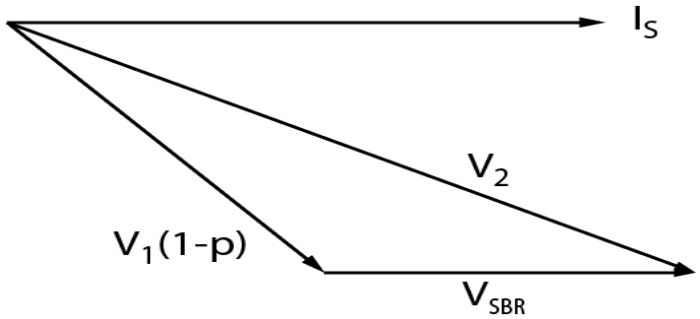

Figure 8: Fresnel representation of the stator voltage, during the fault, with SBR.

The choice of the value of the dynamic resistance is important, a large resistance value will result a large power dissipation, and lower voltages across the rotor. On the contrary, a low-value of the resistors cannot limit the fault current. The dimensioning of the resistance is determined according to two values:

- The resistors must be large enough to limit the rotor voltage to the maximum input voltage tolerated by the converter, thus avoiding its deterioration.

Hence the following condition must be satisfied:

$$e^{r}_{r,max} \leq V_{RSC,max} \tag{39}$$

Since the RSC can only produce a voltage lower than the DC voltage, its maximum output value $V_{RSC,max}$ is calculated as follows:

$$V_{RSC,max} = \frac{V_{dc}}{2\sqrt{\frac{2}{3}}} \tag{40}$$

- The resistors must be small enough to prevent the stator voltage exceeding his maximum voltage value.

During GF, stator voltage can be expressed by the sum of GV and the voltage across the resistors.

$$V_2 = V_1(1-p) + V_{SBR} \tag{41}$$

The voltage V_{SBR} is limited by the maximum stator voltage V_{Smax}, and we have:

$$V_{SBR,max} \leq V_{Smax} - V_1(1-p) \tag{42}$$

Replacing V_{SBR} by $V_{SBR} = R_{SBR}\, I_s$, and we considered the worst case p = 1.
We find:

$$\frac{1}{I_s}\left\{(1-g)V_1 - \frac{M}{L_s}\frac{V_{dc}}{2\sqrt{\frac{2}{3}}}\right\} \leq R_{SDBR} \leq \frac{V_{Smax}}{I_s} \tag{43}$$

4.2 HVRT control strategy

In this section, the capabelity of DFIG using DVR is proved for symmetrical grid VS. When symmetrical grid VS occurs, the DVR control output voltage maintains the stability of the system to avoid the stator and rotor overcurrent and overvoltage. Thus, the power outputs of DFIG are concertedly controlled in order to keep the operation's safety and stability of the grid. The system with the DVR is represented in Figure 9.

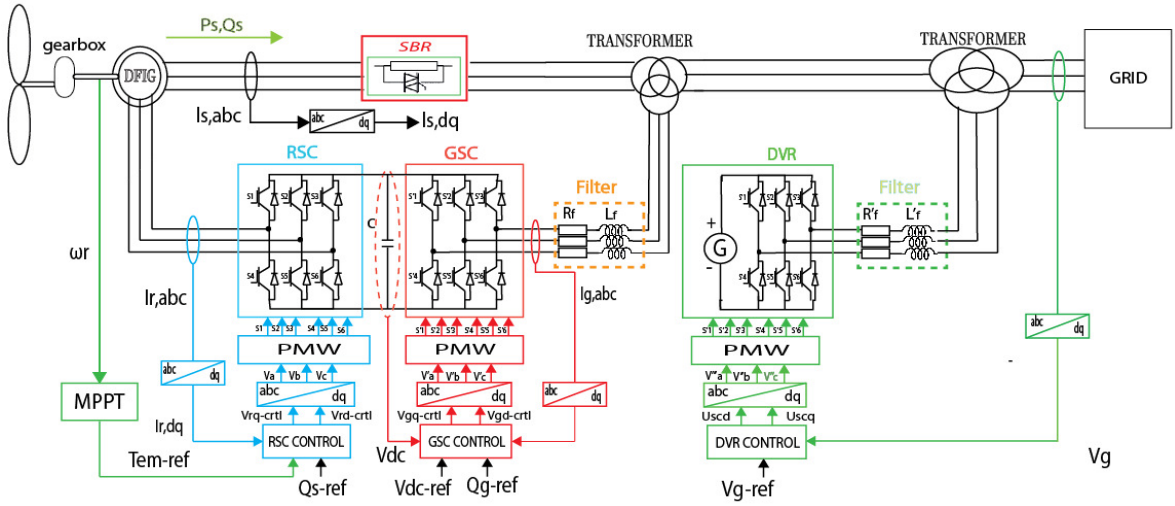

Figure 9: DFIG system with DVR.

a. Dynamic Voltage Restorer control:

The goal of DVR during VSs is to keep the voltage stability on the connection point with the grid, thus, by controlling it to hold the pre-fault state of GV as:

$$V_g' = V_g \tag{44}$$

Where: V_g is the GV during the normal operation; V_g' is the GV during the VSs.
During normal operation, $\boldsymbol{V_g}$ is oriented along d-axix, by DVR control, the voltage at the connection point can be controled to keep the same state befor VSs. GV vector during a VS can be expressed as:

$$\begin{cases} V_g = u_{gd} = V_{gd}' \\ 0 = u_{gq} = V_{gq}' \end{cases} \tag{45}$$

Where: u_{gd} and u_{gq} are stator voltage vector in d-q-axis reference farm during normal operation; V'gd and V'gq are grid voltages respectively d-axis and q-axis component during the fault; Vg is the amplitude of the grid voltage during normal operation, the voltage equations of DVR are expressed as:

$$\begin{cases} u_{gcd} = [Kp_1(\tau_{i1}s + 1)/(\tau_{i1}s)](V_g - V'_{gd}) \\ u_{gcq} = [Kp_1(\tau_{i1}s + 1)/(\tau_{i1}s)](0 - V'_{gq}) \end{cases} \quad (46)$$

Where: Kp1 and τi1 are parameters of the PI controller. According to equation (46), the control block of DVR during GF is shown in Figure 10.

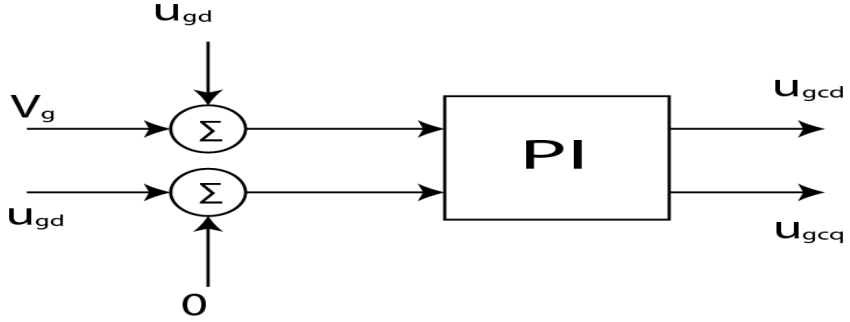

Figure 10: Control diagram of DVR during GV swells.

b. RSC control

In order to improve the HVRT of the DFIG system during VSs, the conventional control strategy for power converter must be changed to avoid the rotor and stator current disturbs and electromagnetic torque oscillations. On the other hand, to stabilize reactive power by controlling power converter. During symmetrical grid VS and by ignoring the stator resistance, the generator active power Ps and reactive power Qs can be written as:

$$\begin{cases} P_s = V_{sq} i_{sq} = V_s i_{sq} \\ Q_s = V_{sq} i_{sd} = V_s i_{sd} \end{cases} \quad (47)$$

From equation (47), in order to keep the same state of active power, q-axis vector of stator current must rest stable, meanwhile, in order to support the grid during VSs by maximizing the absorption of reactive power, d-axis component of stator current must take its maximum value:

$$I_{sdmax} = \sqrt{I_{smax}^2 - I_{sq}^2} \quad (48)$$

Where: $\mathbf{I_{smax}}$ for the stator maximum value. Combined stator flux equation and (48) during a VS, the d-q-axis components of the rotor current expressed:

$$\begin{cases} I_{rd} = \frac{\psi_s}{L_m} - \frac{L_s}{L_m} i_{sdmax} \\ I_{rq} = -\frac{L_s}{L_m} i_{sq} \end{cases} \quad (49)$$

Thus the equations for RSC control block during VS are expressed by:

$$\begin{cases} V'_{rd} = \left[\frac{K_{p2}(\tau_{i2}s+1)}{\tau_{i2}s}\right](I_{rd} - i_{rd}) \\ V'_{rq} = \left[\frac{K_{p2}(\tau_{i2}s+1)}{\tau_{i2}s}\right](I_{rq} - i_{rq}) \end{cases} \quad (50)$$

Where: $\mathbf{V'_{rd}}$ and $\mathbf{V'_{rq}}$ are respectively d and q-axis component of the RSC current loop controller output voltage; $\mathbf{K_{p2}}$ and $\boldsymbol{\tau_{i2}}$ are parameters of the PI controller. The control block of RSC during VS is represented in Figure 11.

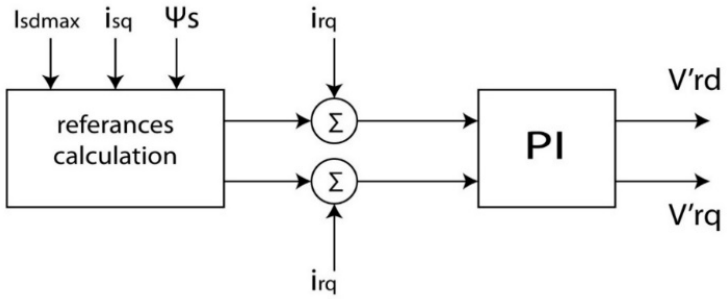

Figure 11: RSC control diagram during grid voltage swells.

c. GSC control

When symmetrical grid VS happens, the GSC is still unchanged for the control of DC link voltage. But when the magnitude of the grid voltage increases, DFIG should absorb reactive power depending to the magnitude of grid voltage swell. When GSC using grid voltage oriented vector control method and ignoring the line resistance $\mathbf{R_g}$, the GSC output voltage is expressed as follow:

$$\begin{cases} U_g = -\omega_s L_g I_{gq} + V_{gd} \\ 0 = \omega_s L_g I_{gd} + V_{gq} \end{cases} \tag{51}$$

Where: U_g is the amplitude of the GV vector; L_g is the line inductance; V_{gd} and V_{gq} are respectively d-axis and q-axis components of the GSC output voltage; I_{gd} and I_{gq} are d-axis and q-axis components of the GSC current.

According to the vector modulation theory, at no over-modulation condition, the modulation ratio m shall meet:

$$m = \left[\frac{\sqrt{V_{gd}^2 + V_{gq}^2}}{\frac{U_{dc}}{2}}\right] \leq 2/\sqrt{2} \tag{52}$$

From equations (51) and (52) we can deduct:

$$V_{dc} \geq \sqrt{3\left[(V_g + \omega_s L_g I_{gq})^2 + (-\omega_s L_g I_{gd})^2\right]} \tag{53}$$

From (53), the minimum reactive current $\mathbf{I_{gqmin}}$required can be expressed as:

$$I_{gqmin} = \frac{1}{\omega_s L_g}\left[\sqrt{\frac{U_{dc}^2}{3} - (-\omega_s L_g I_{gd})^2} - U_g\right] \tag{54}$$

During the grid VSs; to achieve the HVRT requirement, GSC should absorb at least the minimum reactive power $\mathbf{Q_{gmin}}$ as:

$$Q_{gmin} = -I_{qmin} U_g \tag{55}$$

During the fault, GSC reactive power set point is obtained by equation (12), which keep the DC bus voltage value stable at fault time, to guarantee a stable support for each process control.

Thus the equations for current loop control of GSC are:

$$\begin{cases} \mathbf{V'_{gd}} = \left[\frac{\mathbf{K_{p3}(\tau_{i3}s+1)}}{\mathbf{\tau_{i3}s}}\right](\mathbf{I_{gd}} - \mathbf{i_{gd}}) \\ \mathbf{V'_{gq}} = \left[\frac{\mathbf{K_{p3}(\tau_{i3}s+1)}}{\mathbf{\tau_{i3}s}}\right](\mathbf{I_{gq}} - \mathbf{i_{gq}}) \end{cases} \tag{56}$$

The control block of GSC during GF is shown in figure 12.

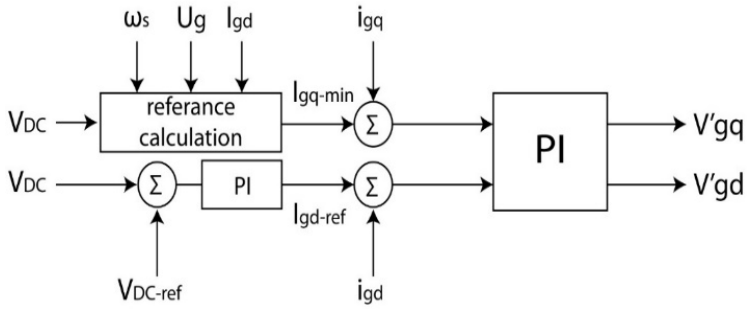

Figure 12: GSC control diagram during grid voltage swells.

4.3 Combining HVRT and LVRT methods:

To ensure a great management of any GF types, we propose a combination strategy between LVRT and HVRT strategies. Figure 13 shows the algorithm of FRT strategy proposed. Through normal operation, GV is measured in real time to look over GFs and its nature. In the meanwhile, a GF is tested by measuring in real time the GV. In addition, during VDs whish passed 30%, the GV measured is between 0,7pu and 0.9pu, only the active method is used (Figure 13, option 1). Thus, in this range, active method is more coherent, and SBR protection is not working. On the other hand, for high VDs higher than 30%, when the GV is less than 30%, only the SBR is used with conventional control (Figure 13, option 2). Moreover, if the VS is more than 10%, the GV measured is higher than 1.1pu, the DVR strategy is activated (Figure 13, option 3) with the proposed control fitting the improvement of the safety and the stability of the grid under VSs. Finely, at time of clearing the fault, the system respond to a normal operation.

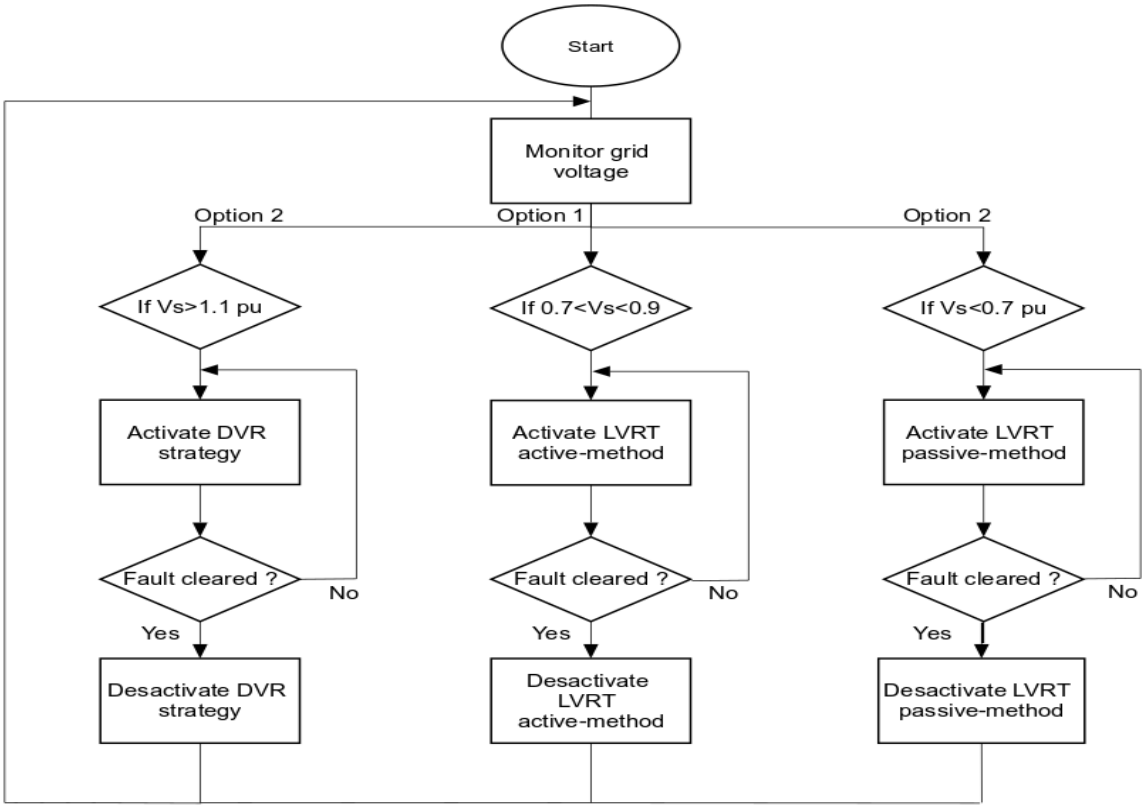

Figure 13: the flowchart of the proposed strategy based on the combination of HVRT and LVRT methods.

5 Simulation & results

The mean work was produced by the simulation results were conducted using MATLAB-SIMULINK software and Simscape SimPowerSysteme toolbox. The DFIG FRT capability is simulated for two types of GF: (i) three-phase VDs in which the grid VD twice to 0.1 pu (10% of its rated value) at t=0.7s and lasts for 150ms, and to 0.75 pu (75% of its rated value) at t=1.2s and lasts for 200ms as shown in figure 14. (ii) three-phase VS in which the GV increase to 1.3 pu at t=0.7 with a duration of 100ms as shown in Figure 16. (the DFIR parameter are given in Table 2)

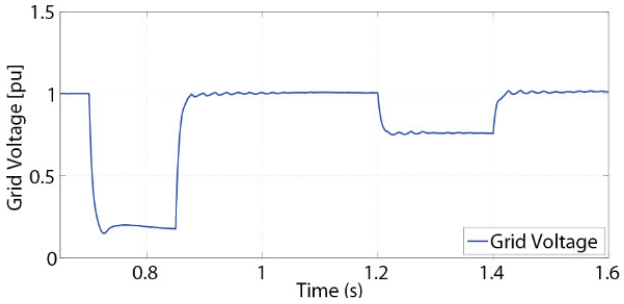

Figure 14: Grid voltage during tow voltage dips.

Figure 15 shows the simulation results of different electric quantities for the system with and without LVRT strategy. The first voltage sag of a GF had started at t=0.7s, in figure 15.(a) through the first 90% VD, the passive method is activated. It is shown that the active power of the system without LVRT technique reaches 0.1pu which exceeded the DFIG operation limit (0,7pu) also, the DFIG is ended. However, with the LVRT advanced method, the active power rest in the garneted operation range (0.7pu – 1.3pu). When the voltage sag is disappeared at 0,85s, the DFIG starts and the active power leads 2.24pu for the system without LVRT technique. Nevertheless, the proposed LVRT method regards the range of normal operation and doesn't notice any active power peak. The next voltage sag is 25%, in this time the active method is operated and the passive method is deactivated. The present results report the efficiency of the proposed approach, it maintain the stability of the production.

In Figure 15.(b) relieve that the combined method considers grid requirements. In fact, the reactive power has to be maintained at least within 0,3pu and 0,4pu. Moreover, the system without LVRT strategy exceeds the limit of the reactive power and can affect the grid.

Figure15.(c) and figure 15.(d) show the simulation results of the electromagnetic torque and the rotor current. It is shown that the system without LVRT strategy has serious oscillations in electromagnetic torque and rotor current, which is very limited near its nominal value by using the SBR. In addition, for a system without LVRT, rotor current passed the permissible value (2pu). Moreover, it is shown that when the fault is started, rotor current has dangerous peaks with strong oscillations, which have an important influence on the performance of the mechanical part of DFIG and the protection of the power converters. Actually, serious oscillations can destroy the machine and the power converter.

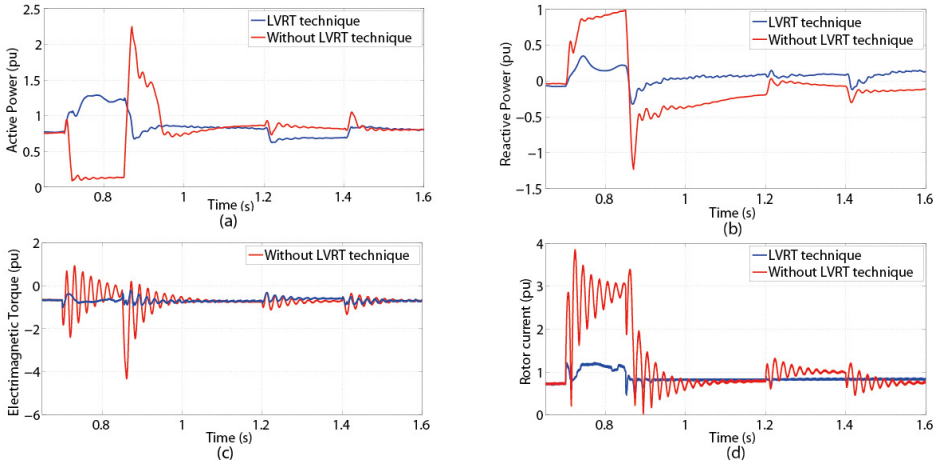

Figure 15: Simulation results of different electric quantities for the system with and without LVRT strategy.

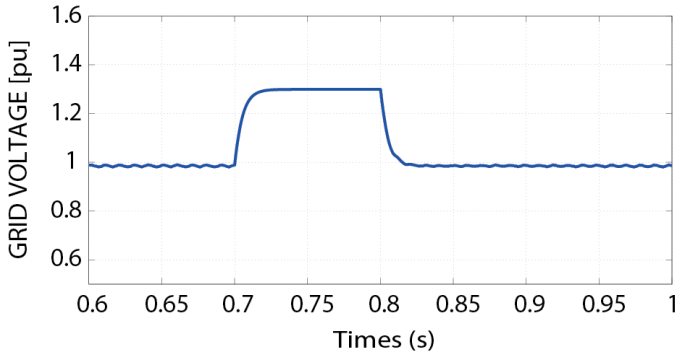

Figure 16: Grid voltage during a voltage swell.

During the grid VSs, Figure 17.(a) show that the amplitude of the stator voltage was remarkably expended with the grid VSs to 1.3pu, which will possibly be harmful to the stator insulation level, but with the proposed strategy, DVR compensates the change in GV, as consequence, the stator voltage holds the pre-fault state. Figure 17 (b) and (c) show that without DVR the rotor and stator over-currents contain a large transient DC component during VSs. Therefore, with the strategy proposed the transient DC component of stator flux could be effectively reduced.

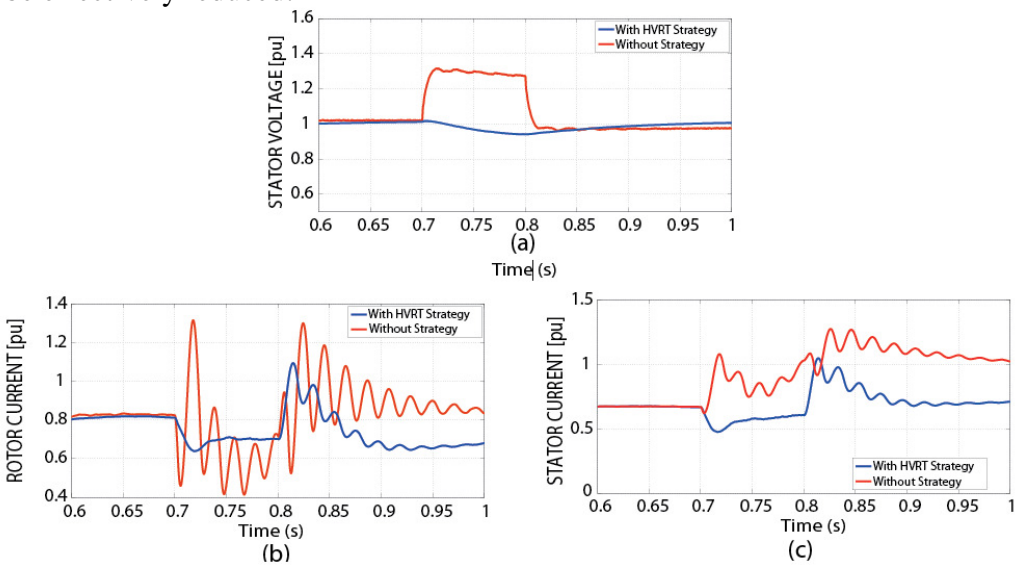

Figure 17: Simulation results of different electric quantities for the system with and without HVRT strategy.

According to Figure 18 (a), (b), (c), the electromagnetic torque, active power and reactive power present significant fluctuations, which will have an impact on mechanical components of DFIG, at the same time significantly reduce grid power quality, but with the proposed strategy, the fluctuations in electromagnetic torque and power output was significantly amortized, in this fact, the impact on the WT will be reduced, in addition the proposed strategy can support grid power quality through the fault. From Figure 18 (d) we remark that the DC-link voltage is almost substantial, by using the proposed strategy which remains the safety and the stability of the DC link.

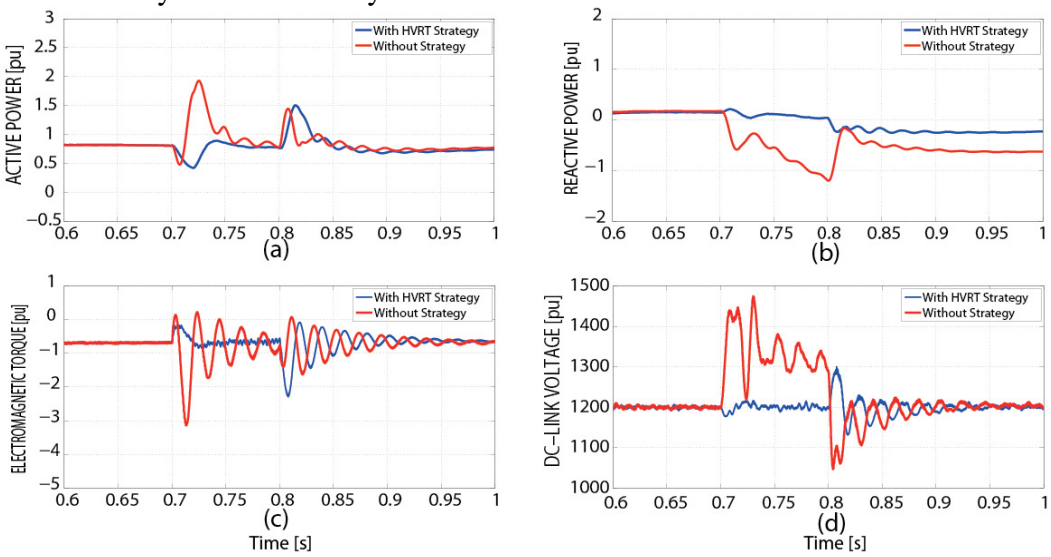

Figure 18: Simulation results of different electric quantities for the system with and without HVRT strategy.

Table 2: DFIG parameters.

Stator (Star connection)	
Rated voltage V_{sn}	575V
The stator resistance R_s	0.023 pu
The stator inductance L_s	3.08 pu
Mutual inductance M_{sr}	2.9pu
Rotor (Star connection)	
Rated voltage V_{rn}	1975V
The rotor resistance R_r	0.016 pu
The rotor inductance L_r	3.06 pu
Mechanical quantities	
Number of pole pairs p	3
Moment of inertia J	$0.685s$
Coefficient of friction f	$0.01pu$

6 Conclusion

The LVRT and HVRT capabilities of WTs are necessary with the increasing integration of wind energy and contribute to the regular grid integration. This paper has investigated the performance of the passive and active methods for FRT capability of DFIG. Hence, The

LVRT strategy is based on the active method which used a P controller that valid only for low VDs less than 30%, also an SBR coupled in series with the stator windings is used for the passive method. Besides, the proposed HVRT strategy is based on adding a DVR, which provides the balance of the GV by controlling the reactive power. The simulation results have been allowed an indication of the proposed method behavior during any voltage faults. Further, the results of the simulation obtained using a 1.5 MW DFIG connected to electrical grid, report the great performance of the proposed strategies for improving the FRT capability of DFIG.

References

[1] MS. Aziz, GM. Mufti 'Wind-hybrid Power Generation Systems Using Renewable Energy Sources-A Review', International Journal of Renewable Energy Research (IJRER), vol 7. No 1. 111-127. 2017.

[2] Ouedraogo, N. S. (2017). Africa energy future: Alternative scenarios and their implications for sustainable development strategies. Energy Policy, 106, 457-471.

[3] Peña Asensio, Andrés, et al. "A Voltage and Frequency Control Strategy for Stand-Alone Full Converter Wind Energy Conversion Systems." Energies 11.3 (2018): 474.

[4] A. Khedher, N. Khemiri 'Wind energy conversion system using DFIG controlled by backstepping and sliding mode strategies' International Journal of renewable energy research (IJRER). vol 2. n3. p 421-430. 2012.

[5] T. R. Ayodele, A. Jimoh, J. L. Munda 'Challenges of grid integration of wind power on power system grid integrity: a review' International Journal of renewable energy research (IJRER). Vol 2. n4. p 618-626. 2012.

[6] Naimi, D., & Bouktir, T. (2008). Impact of wind power on the angular stability of a power system. Leonardo Electronic Journal of Practices and Technologies, 7(12), 83-94.

[7] M. Altin, Ö. Göksu, R. Teodorescu, P. Rodriguez 'Overview of recent grid codes for wind power integration' In: Optimization of Electrical and Electronic Equipment (OPTIM), 12th International Conference on. IEEE. p 1152-1160. 2010.

[8] A. el makrini, Y. el karkri, Y. boukhriss 'LVRT Control Strategy of DFIG Based Wind Turbines Combined the Active and Passive Protections' International Journal of Renewable Energy Research (IJRER). vol 7.n 3. p 1258-1269. 2017.

[9] Reddy, KV Ramana, N. Ramesh Babu, and P. Sanjeevikumar. "A review on grid codes and reactive power management in power grids with wecs." Advances in Smart Grid and Renewable Energy. Springer, Singapore, 2018. 525-539.

[10] P. Kumar, A. K. Singh, 'Grid Codes: Goals and Challenges' Renewable Energy Integration. Springer Singapore. p 17-39. 2014.

[11] R. Perveen, N. Kishor, S. R. Mohanty, 'Off-shore wind farm development: Present status and challenges', Renewable and Sustainable Energy Reviews. vol 29. p 780-792. 2014.

[12] Y. Boukhris, A. El Makrini, H. El Moussaoui, H. El Markhi, 'Low Voltage Ride-through Capability Enhancement of Doubly Fed Induction Generator Based Wind Turbines under Voltage Dips' International Journal of Power Electronics and Drive Systems. vol 6. n4. 2015.

[13] M. Mohsen, 'Dynamic performance assessment of DFIG-based wind turbines: A review, Renewable and Sustainable Energy Reviews' vol 37 .pp 852-866. 2014.

[14] Toumi, S., Amirat, Y., Elbouchikhi, E., Trabelsi, M., Benbouzid, M., & Mimouni, M. F. (2017). A comparison of fault-tolerant control strategies for a PMSG-based marine current turbine system under generatorside converter faulty conditions. Journal of Electrical Systems, 13(3).

[15] Y. Amirat, M.E.H. Benbouzid, B. Bensaker 'Generators for wind energy conversion systems: State of the art and coming attractions' Journal of Electrical Systems. vol 3. n1. pp 26-38. March 2007.

[16] S. Tohidi, P. Tavner, R. McMahon, H. Oraee, M.R. Zolghadri, 'Low voltage ride-through of DFIG and brushless DFIG: Similarities and differences' Electric Power Systems Research. vol 110. pp 64-72, May 2014.

[17] H.T. Jadhav and R. Roy 'A comprehensive review on the grid integration of doubly fed induction generator' International Journal of Electrical Power & Energy Systems. vol 49. pp 8-18. July 2013.

[18] Ganji, E., & Mahdavian, M. (2016). A Controlling Method of DFIG-Based Wind Turbine for Stability Improvement of Power Delivery to the Power Grid. Journal of Electrical Systems, 12(3).

[19] M. Mohseni and S.M. Islam 'Transient control of DFIG-Based wind power plants in compliance with the Australian grid code' IEEE Trans. Power Electronics. vol 27. n2. pp 2813-2824. June 2012.

[20] Yuan, G., & Liang, R. (2017, October). A DFIG wind turbine low-voltage ride-through control strategy based on resynchronization of rotor side converter. In 2017 China International Electrical and Energy Conference (CIEEC) (pp. 351-355). IEEE.

[21] H.T. Jadhav and R. Roy 'A comprehensive review on the grid integration of doubly fed induction generator' International Journal of Electrical Power & Energy Systems. vol 49. pp 8-18. July 2013.

[22] M. Rahimi and M. Parniani 'Efficient control scheme of wind turbines with doubly fed induction generators for low-voltage ride-through capability enhancement' IET Renewable Power Generation. vol 4. n3. pp 242-252. 2010.
[23] M. Rahimi and M. Parniani, 'Low voltage ride-through capability improvement of DFIG-based wind turbines under unbalanced voltage dips' International Journal of Electrical Power & Energy Systems, vol 60. pp 82-95. September 2014.
[24] El Karkri, Yassir, et al. "A comparison between Series Dynamic Resistors and CROWBAR circuit protection for LVRT capability of Doubly-Fed Induction Generator." IOP Conference Series: Earth and Environmental Science. Vol. 161. No. 1. IOP Publishing, 2018.
[25] S.I. Gkavanoudis and C.S. Demoulias 'A combined fault ride through and power smoothing control method for full-converter wind turbines employing supercapacitor energy storage system' Electric Power Systems Research. vol 106. Pp 62-72. January 2014.
[26] D. Ramirez, S. Martinez, F. Blazquez and C. Carrero 'Use of STATCOM in wind farms with fixed-speed generators for grid code compliance' Renewable Energy. vol 37. n1. pp 202-212. January 2012.
[27] P.S. Flannery and G. Venkataramanan 'A fault tolerant doubly fed induction generator wind turbine using a parallel grid side rectifier and series grid side converter' IEEE Trans. Power Electronics. vol 23. n3. pp 1126-1135. May 2008.
[28] L. Teng S. Shiyi P. Malliband, E. Abdi and R.A. McMahon, 'Crowbarless fault ride-through of the brushless doubly fed induction generator in a wind turbine under symmetrical voltage dips' IEEE Trans. Industrial Electronics. vol 60. n7. pp 2833-2841. July 2013.